Probing laser induced metal vaporization by gas dynamics and liquid pool transport phenomena

T. DebRoy, S. Basu, and K. Mundra
Department of Materials Science and Engineering, The Pennsylvania State University, University Park, Pennsylvania 16802

During laser beam welding of many important engineering alloys, an appreciable amount of alloying element vaporization takes place from the weld pool surface. As a consequence, the composition of the solidified weld pool is often significantly different from that of the alloy being welded. Currently there is no comprehensive theoretical model to predict, from first principles, laser induced metal vaporization rates and the resulting weld pool composition changes. The weld pool heat transfer and fluid flow phenomena have been coupled with the velocity distribution functions of the gas molecules at various locations above the weld pool to determine the rates of the laser induced element vaporization for pure metals. The procedure allows for calculations of the condensation flux based on the equations of conservation of mass, momentum and energy in both the vapor and the liquid phases. Computed values of the rates of vaporization of pure metals were found to be in good agreement with the corresponding experimentally determined values. The synthesis of the principles of gas dynamics and weld pool transport phenomena can serve as a basis for weld metal composition control.

I. INTRODUCTION

With the growing acceptance of the industrial lasers for welding, certain specific problems in their use have become apparent. The use of very high power density laser source for welding leads to weld pool temperatures that are often higher than those encountered in most other welding processes and it is well known[1,2] that the temperatures of the molten region can frequently exceed the boiling point. Even at modest power densities, laser welding of many important engineering alloys results in significant changes in composition and properties of the weld metal.[3-6] The problem of composition change is particularly pronounced in the welding of thin sheets[3] where the lasers found most widespread use.

Vaporization of alloying elements from the weld pool involves several transport and kinetic steps. For alloys, the vaporization involves transport of various species from the interior of the weld pool to the surface, phase change at the surface and subsequent transport of the vaporized species from the surface to the bulk gas stream. The liquid phase is very well mixed due to intense Marangoni convection, and the transport of the alloying elements from the interior of the weld pool to its surface does not inhibit vaporization.[7] The rate of vaporization is mainly governed by the desorption of the vaporizing species at the surface and by the subsequent transport of the species from near the surface to the bulk gas stream. Because of its importance, vaporization phenomena in welding have been investigated both experimentally and theoretically. Apart from the examination of the weld metal composition and structure to evaluate the direct effects of vaporization, much of the previous experimental work was based on the *in situ* monitoring of the alloying element vaporization by emission spectroscopy.[8-10] It was found that during welding of stainless steels, the most dominant species in the vapor phase were iron, manganese, nickel and chromium. Eagar and Block-Bolton[11] used calculations based on the Langmuir equation to demonstrate that iron and manganese were the most prominent vapor species in the welding environment. Although the rates calculated by the Langmuir equation are useful for obtaining relative vaporization rates of various alloying elements,[11] under commonly used welding conditions, the calculated vaporization rates are significantly higher than the corresponding experimentally determined vaporization values. Even at low pressures, of the order of 200 micrometers of Hg, the vaporization rates of pure metal drops were found[12] to be about an order of magnitude lower than the values calculated by the Langmuir equation.

During vaporization at low pressures, the vapor density near the molten pool surface is small, and therefore, the condensation of vapor particles on the weld pool surface can be neglected. However, when a metal is irradiated with a very high power density laser beam, a significant amount of vapor condensation can take place and the kinetics of condensation must be taken into account in the calculation of the net vaporization rates. Anisimov[13] calculated the condensation of vapor by solving gas dynamics equations in a thin layer adjacent liquid metal–vapor interface, known as the Knudsen layer. However, the temperature calculations at the surface of the metal were done by using an approximate energy balance which included only the energy used in the vaporization, but completely ignored heat transfer due to conduction and convection. For vaporization of aluminum, Knight[14] derived a set of gas dynamic equations across the Knudsen layer and calculated the fraction of the vaporized material that condenses for a given local surface temperature. Recently, Chan and Majumdar[15] used Knight's equations to calculate laser in-
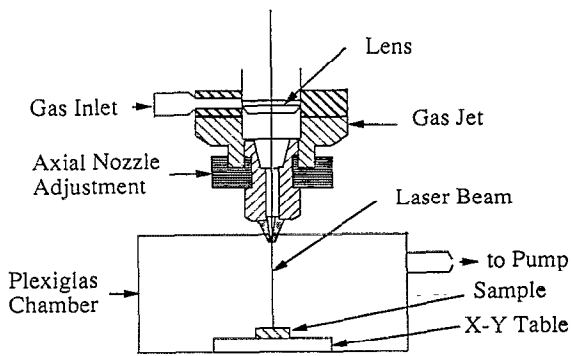
FIG. 1. A schematic diagram of the experimental setup.

duced material vaporization rates from molten aluminum, titanium and a superalloy. In the works of Knight[14] or Chan and Majumdar,[15] the temperature calculations were performed in one dimension. Furthermore, no correlation between the theoretical predictions and the experimental results was attempted in these studies.

The work reported in this paper is aimed at understanding laser induced vaporization of pure metals. Since Anisimov's work[13] was published, significant advancement has been made in the application of transport phenomena for the calculation of weld pool temperature and velocity fields. At present, weld pool temperature calculations are commonly performed by taking into account both heat conduction and Marangoni convection in the weld pool. In the work reported here, the fluid flow and temperature fields in the molten pool were simulated by the solution of the Navier–Stokes equations and equation of conservation of energy. The heat transfer to the shielding gas was taken into account by using a correlation among the various dimensionless numbers. The computed weld pool temperature distribution was then used together with the fundamental principles of gas dynamics and mass transfer for the calculation of the vaporization rates. By using the equations of conservation of mass, momentum and translational kinetic energy across the Knudsen layer, the density and the velocity of the vapor above the liquid–vapor interface and the convective vaporization rates due to total pressure gradients were obtained. In the absence of a total pressure gradient, mass transfer calculations were performed using available correlations amongst various dimensionless numbers. The total vaporization rates were calculated from the local values of vaporization rates for various experimental conditions for ultra pure titanium and iron. The theoretically predicted rates were compared with the corresponding experimentally determined values.

II. EXPERIMENTAL PROCEDURE

A schematic diagram of the experimental set-up is presented in Fig. 1. A carbon dioxide laser, Coherent Model Everlase 525-1 was used. Samples of pure iron and titanium were placed on a remotely controlled, electrically operated table capable of providing linear motion. The samples were irradiated inside a plexiglass box using a 2.54

$\times$ 10^{-1}-m-diam, 0.127-m focal length Zn–Se lens with an antireflection coating. The amount of material lost was determined from the measured values of the loss in sample weight. Furthermore, to obtain precision in measurements, samples were irradiated in several spots so that the weight loss due to vaporization was significant, and samples of small initial weights were used. Argon was used as the shielding gas for all experiments.

III. THEORETICAL CONSIDERATIONS

A. Temperature and velocity profiles for the molten pool

The rate of vaporization from the weld pool is influenced by the temperature distribution at the pool surface. For laser welding, experimental determination of the temperature profile at the weld pool surface is difficult since the pool size is small and it is often covered by an intense plasma[8–10] which interferes with most noncontact temperature measurement procedures. Techniques based on the selective vaporization of alloying elements[4] do not provide adequate spatial resolution of the temperature at the weld pool surface. A recourse is to simulate temperature fields by mathematical modeling. The task involves numerical solution of the Navier–Stokes equations and the equation of conservation of energy. This approach has been adopted in this paper. Since the appropriate equations are well documented in standard textbooks, and the boundary conditions and other details of the application of these equations to welding are available[16–18] in the recent welding literature, these are not presented here. An additional feature in the computational scheme that has been taken into account in the boundary conditions is the heat flux to the shielding gas from the surface of the pool. The local heat flux, J_h is given by

$$J_h = h[T_l - T_g], \tag{1}$$

where T_l is the local weld pool surface temperature, T_g is the ambient temperature and h is the heat transfer coefficient given by the following relation[19] derived from experimental data:

$$h = \frac{2Pr^{0.42}Re^{0.5}k}{d}\left(1 + \frac{Re^{0.55}}{200}\right)^{0.5}$$
$$\times\left(0.483 - 0.108\frac{r}{d} + 7.71\times10^{-3}\left[\frac{r}{d}\right]^2\right), \tag{2}$$

where d is the diameter of the nozzle, r is the radial distance on the pool surface, k is the thermal conductivity of argon at temperature T_{av}, Re is the Reynolds number at the nozzle exit, and Pr is the Prandtl number.

B. Vaporization due to pressure gradient

The velocity distribution functions of the vapor molecules escaping from the weld pool surface at various locations are shown schematically in Fig. 2. Near the weld pool surface, the molecules cannot travel in the negative direction and, as a consequence, the distribution function is half-Maxwellian. Close to the weld pool surface, there ex-
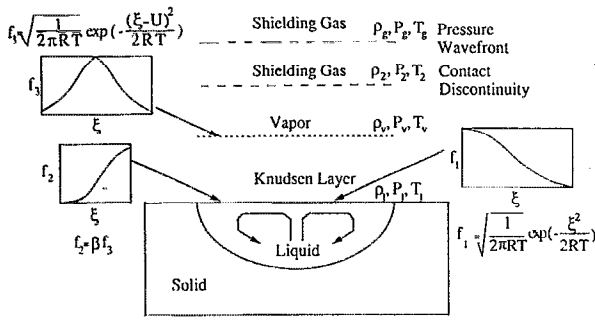
FIG. 2. A schematic diagram of the velocity distribution functions in the Knudsen layer and in adjacent regions.

ists a space of several mean free paths length, known as the Knudsen layer,[13] at the outer edge of which the velocity distribution reaches the equilibrium distribution. Here the vapor molecules can have all possible velocities from $-\infty$ to $+\infty$ as observed in Fig. 2. A portion of the vaporized material condenses on the liquid surface.

The pressure, P_l, at the surface of the molten pool is related to the surface temperature T_l by the Clausius–Clapeyron relationship.

$$\frac{P_l}{P_g} = \exp\left[\frac{M_v L_v}{R T_{lv}}\left(1 - \frac{T_{lv}}{T_l}\right)\right],\qquad (3)$$

where L_v is the latent heat of vaporization, P_g is the equilibrium vapor pressure at a reference temperature, T_{lv}, and M_v is the molecular weight of the vapor.

The temperature T_v, density ρ_v, pressure P_v and the mean velocity of the vapor, u, at the edge of the Knudsen layer can be related to T_l, P_l, and ρ_l, the density of the vapor at the liquid surface, by treating the Knudsen layer as a gasdynamic discontinuity. Anisimov[13] and Knight[14] derived expressions for the changes in the vapor density, temperature, velocity and the extent of condensation by using the velocity distribution functions presented in Fig. 2 and solving the equations of conservation of mass, momentum, and translational kinetic energy across the Knudsen layer. Since the details of the procedure are available in their papers, only a summary of their results, commonly referred to as the jump conditions, are presented in Eqs. (4)–(6).

$$\frac{T_v}{T_l} = \left[\sqrt{1 + \pi\left(\frac{\gamma_v - 1}{\gamma_v + 1}\frac{m}{2}\right)^2} - \sqrt{\pi}\frac{\gamma_v - 1}{\gamma_v + 1}\frac{m}{2}\right]^2,\qquad (4)$$

where $m = u/\sqrt{2R_v T_v}$, $R_v = R/M_v$ and γ_v is the ratio of specific heats for the vapor which is treated as a monoatomic gas.

$$\frac{\rho_v}{\rho_l} = \sqrt{\frac{T_l}{T_v}}\left((m^2 + 1/2)e^{m^2}\mathrm{erfc}(m) - \frac{m}{\sqrt{\pi}}\right)$$
$$+ \frac{1}{2}\frac{T_l}{T_v}[1 - \sqrt{\pi}m e^{m^2}\mathrm{erfc}(m)],\qquad (5)$$

where erfc is the complimentary error function. The density, ρ_l can be computed from P_l and T_l, assuming that the vapor behaves like an ideal gas. The condensation factor, β, is given by

$$\beta = \left((2m^2 + 1) - m\sqrt{\pi\frac{T_l}{T_v}}\right)e^{m^2}\frac{\rho_l}{\rho_v}\sqrt{\frac{T_l}{T_v}}.\qquad (6)$$

Since there are four unknowns in Eqs. (4)–(6), viz T_v, ρ_v, β, and m, it is necessary to have an additional equation to have unique values of these variables. The necessary equation is obtained by relating the pressure at the edge of the Knudsen layer to the ambient conditions. Across the Knudsen layer the vapor wavefront moves into the shielding gas, as shown in Fig. 2. The moving interface between the vapor and the shielding gas is a contact discontinuity. Across this discontinuity the pressures are the same i.e., $P_2 = P_v$. The pressure rise at the liquid vapor interface propagates as a pressure wave. The wavefront may be treated as a pressure discontinuity, and the pressure change across the wavefront may be obtained by applying the Rankine–Hugoniot relation.[20]

$$\frac{P_l}{P_g}\frac{P_2}{P_l} = 1 + \gamma_g M\Gamma\left[\frac{\gamma_g + 1}{4}M\Gamma + \sqrt{1 + \left(\frac{\gamma_g + 1}{4}M\Gamma\right)^2}\right],\qquad (7)$$

where P_g and P_2 are the pressures in front of and behind the wavefront respectively, γ_g is the ratio of specific heats for shielding gas, $\Gamma = \sqrt{\gamma_v R_v T_v}/\sqrt{\gamma_g R_g T_g}$, $R_i = R/M_i$, where M_i is the molecular weight. The Mach number M is related to m according to the equation

$$m = M\sqrt{\gamma_v/2}.\qquad (8)$$

In Eq. (7), P_l/P_g can be computed from Eq. (3) for a given local surface temperature, and since $P_2 = P_v$, for an ideal gas, P_2/P_l can be expressed as a function of m with the help of Eqs. (4) and (5). Thus, Eq. (7) is effectively reduced to a nonlinear equation in m and can be solved iteratively or graphically to obtain m and the Mach number for a given local weld pool surface temperature. The values of T_v, ρ_v, and β, corresponding to a local temperature T_l can be determined from Eqs. (4)–(6) by using the computed value of m. The Mach number and the density ρ_v can then be used to calculate the convective vaporization flux in gms/cm^2 s, J_c corresponding to a local surface temperature T_l due to pressure gradient.

$$J_c = \rho_v M S,\qquad (9)$$

where S is the speed of sound at temperature T_v.

C. Vaporization due to concentration gradient

The diffusive vaporization rate is expressed in terms of a phase change at the surface and the subsequent transport of the vaporized species to the bulk gas phase through the mass transfer boundary layer surrounding the pool. The vaporization rate, in gms/cm^2 s, is then defined as

$$J_d = k_g(M_v/R)(P_l/T_l),\qquad (10)$$

Velocity Field

Vector Scale ——— 100 cm/sec.
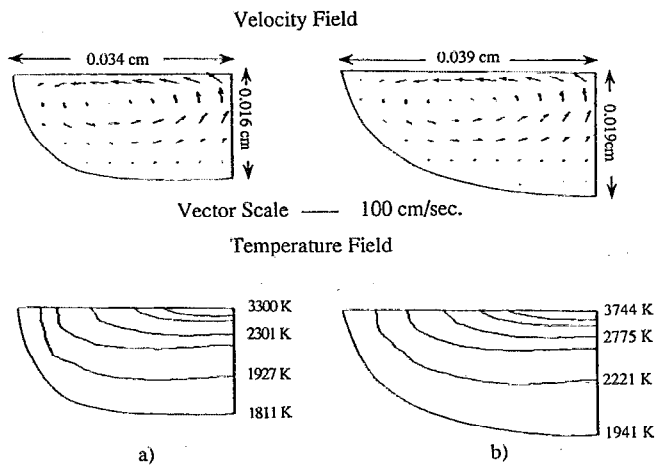
Temperature Field

a)   b)

FIG. 3. Velocity and temperature fields for (a) iron and (b) titanium for a laser power of 500 W and argon flow rate of 1 ℓ/min.

where P_l is pressure in atmosphere, M_v is the molecular weight, R is gas constant in cm^3 atm/gm mole K and k_g is the mass transfer coefficient[19] in cm/s and is given by Eq. (11).

$$K_g = \frac{2Sc^{0.42}Re^{0.5}D}{d}\left(1 + \frac{Re^{0.55}}{200}\right)^{0.5}$$
$$\times \left(0.483 - 0.108\frac{r}{d} + 7.71\times10^{-3}\left[\frac{r}{d}\right]^2\right), \quad (11)$$

where d is the diameter of the nozzle, r is the radial distance on the pool surface, D is the diffusivity of the element in argon at temperature T_{av}, Re is the Reynolds number at the nozzle exit, and Sc is the Schmidt number.

IV. RESULTS AND DISCUSSION

A. Velocity and temperature fields

When a laser beam strikes the surface of the sample, melting occurs almost instantaneously. For a high power density laser beam, the time required to reach the steady

TABLE I. Data used for calculations.

Property	Iron	Titanium
Molecular weight (gm/mole)	55.85	47.9
Density (gm/cm³)	7.8	4.54
Melting point (K)	1811.0	1941.0
Boiling point (K)	3135.0	3533.0
$d\gamma/dT$ (dyne/cm K)	− 0.5	− 0.26
Latent heat of vaporization (cal/gm)	1514.02	2110.08
Latent heat of melting (cal/gm)	70.0	96.298
Thermal conductivity of solid (cal/cm s K)	0.045	0.049
Thermal conductivity of liquid	0.10	0.12
Specific heat of solid (cal/gm K)	0.168	0.177
Specific heat of liquid (cal/gm K)	0.197	0.187
Effective viscosity (gm/s cm)	0.8	0.5
Ratio of specific heats of vapor (γ_v)	1.667	1.667
Absorption coefficient	0.15	0.2

TABLE II. Experimental and theoretical depth and diameter of the laser melted pool for titanium and iron for a laser power of 500 W and gas flow rate of 1 ℓ/min.

Element	Iron		Titanium	
Depth/diam	Experimental	Theoretical	Experimental	Theoretical
Diam (cm)	7.0×10^{-2}	6.8×10^{-2}	8.0×10^{-2}	7.8×10^{-2}
Depth (cm)	1.7×10^{-2}	1.6×10^{-2}	2.0×10^{-2}	1.9×10^{-2}

state is very small. Zacharia et al.[22] noted that in laser welding "quasisteady" state is achieved very quickly as the energy supplied to the weld pool is rapidly conducted away by the base metal. Mehrabian et al.[23] showed that the time required to reach the maximum melt depth for iron for a laser power of 2×10^5 watts/cm² is of the order of 1 ms. Thus, for much of the duration of a large laser pulse of several milliseconds span, the molten pool is in a steady state. The steady state temperature and velocity fields, calculated from the solution of Navier–Stokes equation and the equations of conservation of mass and energy are shown in Fig. 3. The calculation takes into consideration the heat loss to the argon shielding gas. The data used for the calculations are presented in Table I. The details of the calculations of thermal conductivity and viscosity of the shielding gas used in the calculations are described in the Appendix. The laser beam absorption coefficient for iron was taken from the data of Khan and DebRoy,[24] and the absorption coefficient value for titanium was calculated using Bramson's empirical relation.[25] Both iron and titanium have a negative temperature coefficients of surface tension. Therefore, the velocities at the surface are radially outwards resulting in a relatively shallow pool. The maximum radial velocities are of the order of 60 cm/s which is close to the value reported by Zacharia et al.[22] The temperature profiles indicate that there is a strong temperature gradient on the surface of the pool consistent with the absorption of a significant amount of energy in a small localized area near the laser beam axis. The experimentally determined weld pool diameter and depth are compared with the corresponding theoretically predicted values in Table II. It is observed that there is good agreement between the experimental and the calculated values. For the same power, the larger liquid pool size of titanium is consistent with its higher laser beam absorption coefficient.

B. Vaporization rates

The calculated values of the radial distribution of temperature in the liquid pool for iron and titanium are presented in Fig. 4. From the data it is evident that in each case, there is a region on the surface of the molten pool where the temperatures are greater than the boiling point. Liquid pool surface temperatures in excess of boiling point have been reported by several authors. For example, von Allmen[26] determined molten pool temperatures in excess of the boiling point for laser treatment of copper. Batanov et al.[27] indicated that the temperatures on the surface of the laser irradiated material can be higher than the normal boiling point of the material. Theoretical calculations of
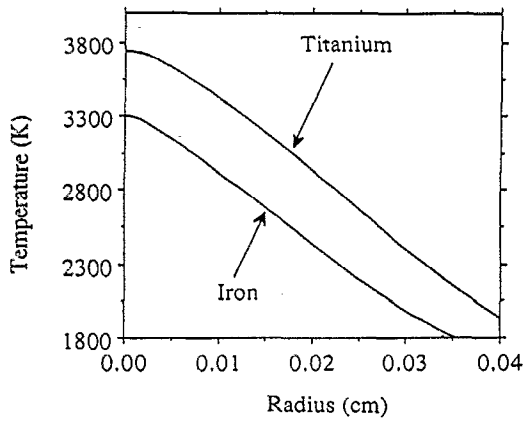
FIG. 4. Computed liquid pool surface temperature for iron and titanium at a laser power of 500 W and gas flow rate of 1 ℓ/min.
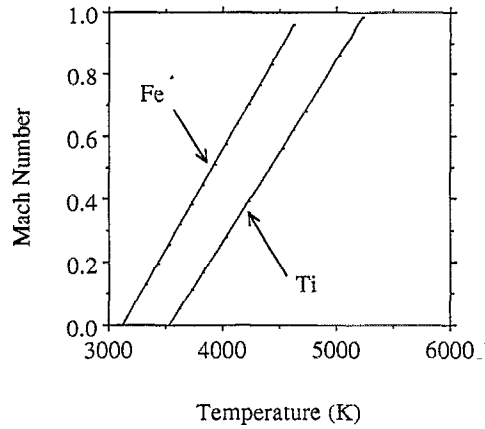

FIG. 6. Mach number for iron and titanium for different temperatures at the edge of Knudsen layer.

the vaporization rates by Knight[14] and Anisimov[13] are based on the premise that the liquid pool surface temperatures are higher than the boiling point. Paul and Deb-Roy[16] and Zacharia et al.[22] have reported temperatures close to the boiling point for laser welding. Khan and Deb-Roy[4] calculated liquid pool surface temperatures from the ratio of the rates of vaporization of alloying elements and reported that the temperature at the center of the weld pool was close to the boiling point. Chan and Majumdar[15] have also been reported temperatures greater than the boiling point for the laser irradiation of aluminum, titanium and a superalloy.

At temperatures in excess of the boiling point, the high vapor density near the surface of the pool leads to significant condensation of the vapor on the surface and the vaporization rate is determined by the conditions across the Knudsen layer. In such a case, the relations among the temperature, pressure and the Mach number for a material can be represented on a plot temperature versus pressure for the various values of Mach number. The plot, commonly referred to as the flow state diagram, obtained from the solution of Eqs. (3)–(8) for iron is shown in Fig. 5. For a given local weld pool surface temperature, the equilibrium vapor pressure can be calculated from the Clausius–Clapeyron relation. The Mach number of the vapor across the Knudsen layer is then uniquely defined and is given by the Mach number of the line that intersects the Clausius–Clapeyron curve at that temperature. The density of the vapor across the Knudsen layer is then calculated by making use of Eq. (5). The calculated values of the Mach number and the density of the vapor across the Knudsen layer as a function of surface temperature are presented in Figs. 6 and 7, respectively. When the relative vaporization behavior of iron and titanium are compared, convective vaporization due to pressure gradient is observed to be dominant at lower temperatures for iron. This is due to the fact that iron has a lower boiling point as compared to titanium. Between the two metals, the relatively higher vapor pressure of iron at any given temperature is reflected in higher Mach number and higher vapor density as can be observed from Figs. 6 and 7.
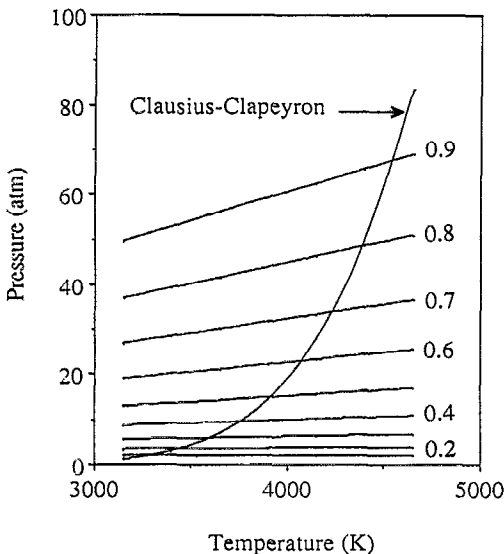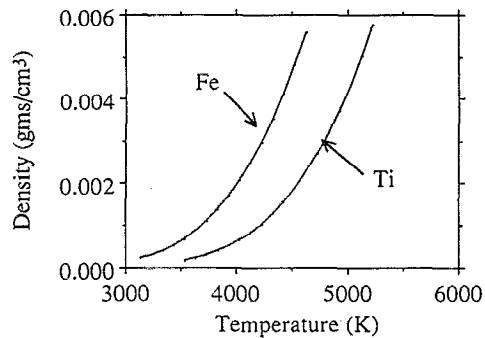

FIG. 5. Flow state diagram for iron.

FIG. 7. Density of iron and titanium vapors for different temperatures at the edge of the Knudsen layer.
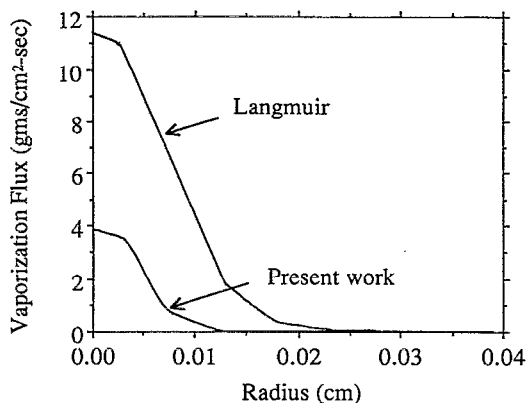
FIG. 8. Vaporization flux of iron calculated from Langmuir equation and from the model presented in this paper for a laser power of 500 W and gas flow rate of 1 ℓ/min.

At temperatures lower than the boiling point, the rate of vaporization is computed from mass transport considerations which takes into account the gas flow conditions and the nature of the shielding gas. In order to determine the mass transfer coefficient, the diffusivity of iron and titanium in the shielding gas and the viscosity of the shielding gas were determined by making use of the Chapman–Enskog theory.[21] The details of the estimation procedure are given in the Appendix. The partial pressures of the metal vapors in the bulk gas stream away from the weld pool surface is negligible as compared to their values at the gas–liquid interface. The radial distribution of the vaporization flux calculated from Eqs. (9) and (10) and from the Langmuir equation are plotted in Figs. 8 and 9 for iron and titanium, respectively. It is observed that the rates predicted by the Langmuir equation are always higher than the actual rates. The total vaporization rate obtained from the integration of the local flux over the entire pool surface, the integrated local Langmuir fluxes and the experimentally determined rate are plotted in Fig. 10 for both titanium and iron. It is observed that the rates predicted by the model are in good agreement with the corresponding ex-

FIG. 10. Comparison of the experimental vaporization rate with the rates calculated from the Langmuir equation and from the model presented in this paper for a laser power of 500 W and gas flow rate of 1 ℓ/min.

perimental data. Furthermore, the vaporization rates predicted by the Langmuir equation are much higher than the experimentally determined rates.

Collur et al.[7] measured vaporization rates during laser welding of AISI 201 stainless steel at various shielding gas flow rates and found that the vaporization rate did not change significantly with the gas flow rate. Our calculations indicate that with the increase in the gas flow rate, there is no significant change in the temperature distribution at the pool surface as can be observed from Fig. 11 and the vaporization rate does not change with shielding gas flow rate. The calculated vaporization rates are consistent with the experimental observations made by Collur et al.,[7] as can be observed from Fig. 12.

V. CONCLUSIONS

Laser induced vaporization rates predicted from the principles of gas dynamics and weld pool transport phenomena are shown to be in good agreement with the corresponding experimental values for the vaporization of iron and titanium. The weld pool surface temperature profiles were simulated from the solution of the equations of conservation of heat, mass and momentum. The computed values of the weld pool width and depth were in good agreement with the corresponding experimentally deter-
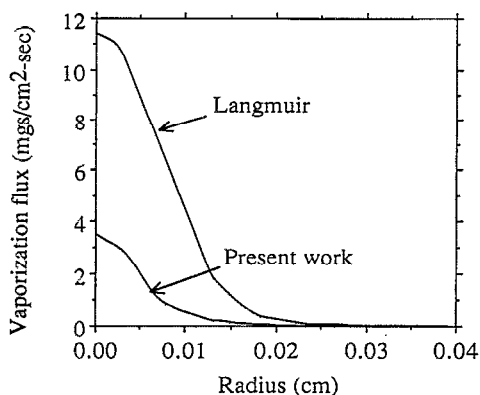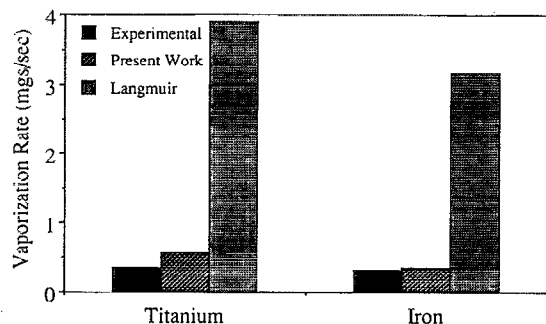

FIG. 9. Vaporization flux of titanium calculated from Langmuir equation and from the model presented in this paper for a laser power of 500 W and gas flow rate of 1 ℓ/min.
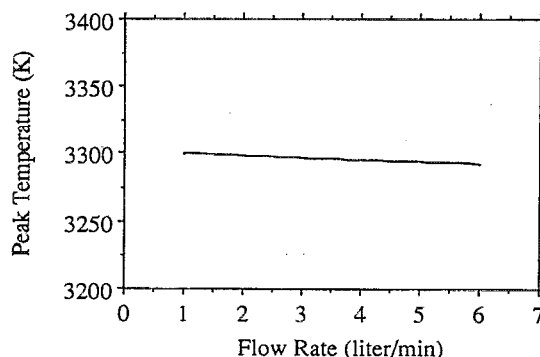

FIG. 11. Peak temperatures calculated as a function of gas flow rate for iron at a laser power of 500 W.
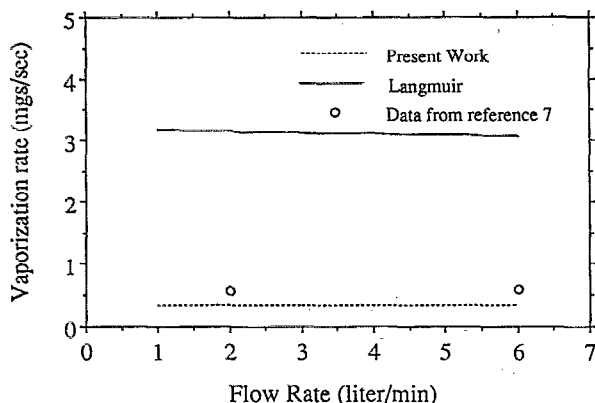
FIG. 12. Vaporization rate as predicted from the model and from the Langmuir equation for iron for different flow rates of argon shielding gas. Also plotted in the figure are the experimental vaporization rates of *AISI 201* steel obtained from Ref. 7.

mined values. Vaporization rates predicted by the Langmuir equation were found to be much higher than the corresponding experimental values for both titanium and iron. Independent experimental results on the effect of shielding gas flow rate on the vaporization rate could be explained on the basis of the model for the laser induced vaporization presented in this paper.

ACKNOWLEDGMENT

APPENDIX

The thermal conductivity of argon which depends on the absolute temperature is given by

$$k_{Ar} = [1.9891 \times 10^{-4}/\sigma^2_{Ar}\Omega_k(T^*)] T/M_{Ar},$$

where σ is the collision diameter in angstrom, $T^* = k_B T/\epsilon$ where k_B is the Boltzmann constant, ϵ is the intermolecular force parameter and Ω_k is the slowly varying function of the dimensionless parameter kT/ϵ.

The viscosity of argon at temperature T is given by

$$\mu_{Ar} = [2.6693 \times 10^{-5}/\sigma^2_{Ar} \Omega_\mu(T^*)] \sqrt{M_{Ar}T},$$

where Ω_μ is again a slowly varying function of the dimensionless parameter kT/ϵ.

The mass diffusivity of titanium and iron in argon, D_{A-Ar}, at absolute temperature T is given by

$$D_{A-Ar} = \frac{0.001\,858\,3 \sqrt{\left(\frac{1}{M_A} + \frac{1}{M_{Ar}}\right) T^3}}{\sigma^2_{A-Ar} \Omega_{D,A-Ar}T^*)},$$

TABLE III. Data used for calculation of heat and mass transfer coefficients.

Parameter	Iron	Titanium	Argon
σ (A)	2.43	2.76	3.418
ϵ/k	3541.185	3894.83	124.0

where M_A is the molecular weight of titanium or iron, $\sigma_{A-Ar} = (\sigma_A + \sigma_{Ar})/2$, $\Omega_{D,A-Ar}$ is a slowly varying function of kT/ϵ_{A-Ar} where

$$\epsilon_{A-Ar} = \sqrt{(\epsilon)_A(\epsilon)_{Ar}}.$$

The data used for the calculation of the various parameters are given in Table III. The values of Ω's were obtained from Ref. 21.

[1] S. I. Anisimov, A. M. Bonch-Bruevich, M. A. El'yashevich, Ya. A. Imas, N. A. Pavlenko, and G. S. Romanvov, Sov. Phys. Tech. Phys. 11, 945 (1967).

[2] F. W. Dabby and U. Paek, IEEE J. Quantum Electron. QE-8, 106 (1972).

[3] P. A. A. Khan, T. DebRoy and S. A. David, Welding Journal 67, 1s (1988).

[4] P. A. A. Khan and T. DebRoy, Metall. Trans. B 15B, 641 (1984).

[5] M. J. Cieslak and P. W. Fuerschbach, Metall. Trans. B 19B, 319 (1988).

[6] T. DebRoy, Trends in Welding Research, edited by S. A. David and J. M. Vitek (ASM Materials Park, OH, 1990), p. 347.

[7] M. M. Collur, A. Paul and T. DebRoy, Metall. Trans. B 18B, 733 (1987).

[8] R. Miller and T. DebRoy, J. Appl. Phys. 68 2045 (1990).

[9] M. M. Collur and T. DebRoy, Metall. Trans. B 20B, 277 (1989).

[10] G. J. Dunn, C. D. Allemand, and T. W. Eager, Metall. Trans. A 17A, 1851 (1986).

[11] A. Block-Bolten and T. W. Eager, Metall. Trans. B 15B, 461 (1984).

[12] P. Sahoo, M. M. Collur, and T. DebRoy, Metall. Trans. B 19B, 967 (1988).

[13] S. I. Anisimov and A. Kh. Rakhmatulina, JETP 37, 441 (1973).

[14] C. J. Knight, AIAA J. 17, 519 (1979).

[15] C. L. Chan and J. Mazumder, J. Appl. Phys. 62, 4579 (1987).

[16] A. Paul and T. DebRoy, Metall. Trans. B 19B, 851 (1988).

[17] G. M. Oreper and J. Szekely, J. Fluid Mech. 147, 53 (1984).

[18] T. Zacharia, A. H. Eraslan and D. K. Aidun, Welding J. 66, 18s (1988).

[19] E. U. Schlunder and V. Ginielinski, Chem. Ing. Tech. 39, 578 (1967).

[20] W. Vincenti and C. Kruger, Introduction to Physical Gas Dynamics (Wiley, New York, 1965).

[21] J. O. Hirschfelder, C. F. Curtiss, and R. B. Bird, Molecular Theory of Gases and Liquids (Wiley, New York, 1954).

[22] T. Zacharia, S. A. David, J. M. Vitek, and T. DebRoy, Welding J. 68, 499s (1989).

[23] R. Mehrabian, S. Kou, S. C. Hsu, and A. Munitz, AIP Conference Proceedings (MRS, Boston, 1978).

[24] P. A. A. Khan and T. DebRoy, Metall. Trans. 16B, 853 (1985).

[25] M. Bramson, Infrared Radiation: A Handbook for Applications, (Plenum, New York, 1968), p. 127.

[26] M. von Allmen, Laser-Beam Interactions with Materials (Springer, 1987), p. 161.

[27] V. A. Batanov, F. V. Bunkin, A. M. Prokhorov, and V. B. Fedorov, Sov. Phys. JETP 36, 311 (1973).

1319   J. Appl. Phys., Vol. 70, No. 3, 1 August 1991

DebRoy, Basu, and Mundra   1319